NASA TM X-27

/N-62

p 34

TECHNICAL MEMORANDUM

X - 27

EFFECTS OF OUTBOARD THICKENED AND BLUNTED LEADING

EDGES ON THE WAVE DRAG OF A 45° SWEPT-WING

AND BODY COMBINATION

By George H. Holdaway, Frank A. Lazzeroni, and
Elaine W. Hatfield

Ames Research Center
Moffett Field, Calif.

CLASSIFICATION CHANGE TO UNCLASSIFIED

AUTHORITY: NASA TECHNICAL PUBLICATION
ANNOUNCEMENT NO. 4

EFFECTIVE DATE: JULY 11, 1961

NATIONAL AERONAUTICS AND SPACE ADMINISTRATION

WASHINGTON   August 1959

NATIONAL AERONAUTICS AND SPACE ADMINISTRATION

TECHNICAL MEMORANDUM X-27

EFFECTS OF OUTBOARD THICKENED AND BLUNTED LEADING

EDGES ON THE WAVE DRAG OF A 45° SWEPT-WING

AND BODY COMBINATION*

By George H. Holdaway, Frank A. Lazzeroni, and
Elaine W. Hatfield

SUMMARY

An investigation to evaluate the effects of thickened and blunted leading-edge modifications on the wave drag of a swept wing has been made at Mach numbers from 0.65 to 2.20 and at a Reynolds number of 2,580,000 based on the mean aerodynamic chord of the basic wing. Two leading-edge designs were investigated and they are referred to as the thickened and the blunted modifications although both sections had equally large leading-edge radii. The thickened leading edge was formed by increasing the thickness over the forward 40 percent of the basic wing section. The blunted modification was formed by reducing the wing chords about 1 percent and by increasing the section thickness slightly over the forward 6 percent of the basic section in a manner to keep the wing sweep and volume essentially equal to the respective values for the basic wing. The basic wing had an aspect ratio of 3, a leading-edge sweep of 45°, a taper ratio of 0.4, and NACA 64A006 sections perpendicular to a line swept back 39.45°, the quarter-chord line of these sections.

Test results indicated that the thickened modification resulted in an increase in zero-lift drag coefficient of from 0.0040 to 0.0060 over values for the basic model at Mach numbers at which the wing leading edge was sonic or supersonic. Although drag coefficients of both the basic and thickened models were reduced at all test Mach numbers by body indentations designed for the range of Mach numbers from 1.00 to 2.00, the greater drag of the thickened model relative to that of the basic model was not reduced. The blunted model, however, had less than one quarter of the drag penalty of the thickened model relative to the basic model at supersonic leading-edge conditions $(M \geq \sqrt{2})$.

---

*Title, Unclassified

INTRODUCTION

The investigation of reference 1 illustrated how a leading-edge modification to a 45° swept wing was effective in improving the wing characteristics at low speeds through maintaining attached air flow on the upper surface of the wing at high angles of attack. The modifications consisted of an increased leading-edge thickness distribution and slight forward camber. However, tests at supersonic speeds, also reported in reference 1, indicated that the modification resulted in an increase in wave drag relative to the basic wing. A similarly modified wing, but without camber, was investigated at transonic speeds with favorable results as reported in reference 2. Thus the major wave-drag penalty of the modification occurs at the higher Mach numbers when the velocity component normal to the wing leading edge is supersonic. For this condition and a blunt leading edge, linearized wave-drag theory is not expected to apply, thereby making experimentation more essential.

An analysis is presented in reference 3 of the low- and high-speed data for various leading-edge contours for swept wings, including the results of references 1 and 2. Low-speed data of reference 3 showed that an outboard concentration of increased leading-edge thickness would yield most or all of the characteristic low-speed benefit, and it was suggested that such an outboard concentration might reduce, or even eliminate, the wave-drag penalty. Accordingly, one of the purposes of the present investigation was to determine whether this was the case. The basic wing-body configuration selected for testing was the same as that for references 1 and 2 and for pertinent tests of reference 3. The modified spanwise variation of leading-edge section initially selected for testing was the same as that designated cut 1 in reference 3. This varying contour of the leading edge will be designated the thickened modification in this report. The wing with this contour had greater volume than the basic wing, but this is not a requirement of the design concepts discussed in reference 3. Thus a wing was designed with essentially the same outboard dimensionless leading-edge radius as for the thickened design but with a volume essentially equal to that of the basic wing. This latter design will be designated the blunted modification in this report. It was formed by reducing the wing chords about 1 percent and concentrating the increased section thickness both outboard and over only a short chordwise extent. In reference 3, a very similar design for a certain high-lift configuration yielded virtually the same low-speed benefit as a full-span modification. (Such a design would probably not yield the full benefit for a wing without leading-edge flaps, see ref. 1.)

Additional objectives of the present investigation were concerned with body indentation. To investigate the possibility that indentation might reduce the wave-drag penalty of the thickened design, separate indentations were designed for the wing of that contour and for the basic wing. These indentations were designed as average shapes for the range

of Mach numbers from 1.00 to 2.00 in a manner similar to that suggested in reference 4. Thus, an additional objective was to evaluate this type of indentation. Finally, it was desired to compare theoretical and experimental wave-drag coefficients, to determine particularly whether computations based on linearized theory could find empirical justification at the supersonic-leading-edge condition. As mentioned previously, theory is not applicable to such flows when the leading edge has any degree of bluntness.

SYMBOLS

b	model span
c	local chord of basic wing measured parallel to the plane of symmetry
c'	local chord of the basic wing design sections measured perpendicular to the 39.45° sweep line (the quarter-chord line of these sections)
$\bar{c}$	mean aerodynamic chord
C_D	drag coefficient
C_{D_b}	base drag coefficient
C_{D_O}	zero-lift drag coefficient
$\left(\Delta C_{D_O}\right)_w$	zero-lift wave drag coefficient
C_{D_f}	estimated friction-drag coefficient
$\left(\Delta C_{D_O}\right)_f$	zero-lift drag coefficient attributed to fixing transition
$\left(\Delta C_{D_O}\right)_{mod}$	zero-lift drag coefficient attributed to leading-edge modifications
C_L	lift coefficient
C_m	pitching-moment coefficient about $\bar{c}/4$ of the basic wing
l	closed-body length

$\dfrac{L}{D}$ lift-drag ratio

$\left(\dfrac{L}{D}\right)_{max}$ maximum lift-drag ratio

L.E. leading edge

M free-stream Mach number

N number of harmonics used in the theoretical computations of wave drag

R Reynolds number

S cross-sectional area perpendicular to body center line

t local wing thickness

x conventional body axis or distance from the wing leading edge to a point in the wing-chord plane measured in the conventional x direction

x' distance from the wing leading edge to a point in the wing-chord plane measured along c'

α angle of attack

η distance measured in the spanwise direction in ratio with the semispan

MODELS

Geometric details of the three wings and the three bodies of revolution tested are presented in tables I and II, and in figure 1. Each wing was tested with a basic body (Sears-Haack body with minimum transonic wave drag for prescribed volume and length) with a closed-body fineness ratio of 12.5. The basic wing and the wing with the thickened leading-edge modification were also tested with indented bodies, which were first designed as a supersonic area-rule shape for each of 21 Mach numbers and then these shapes were averaged over the range of Mach numbers (M = 1.00 to 2.00). This procedure was suggested in reference 4. The wing sections at the tip and the theoretical root or center line of the three wings are shown in dimensionless form in figure 2.

The wing with the thickened modification had the same plan form as the basic wing. For the outer 45 percent of the wing span (as measured

along the leading edge) the sections shown in figure 2 for the thickened modification were constant, while the inboard regions were formed by straight-line elements along constant percent chord lines to give considerably thinner leading-edge sections at the root. The line of discontinuity was perpendicular to the $c'/4$ line. This wing modification was designated cut 1 in reference 3.

The wing with the blunted modification was designed to give the outboard sections bluntness without appreciably altering the volume or plan form of the basic wing. The thickness distribution for this wing is indicated in figures 2 and 1(b). For the outer 40 percent of the wing span, the sections were constant and had the same dimensionless leading-edge radius as the thickened modification. For the inner 40 percent the sections were essentially shortened basic-wing sections with dimensionless leading-edge radius equal to the basic-wing section. The middle sections of this wing were formed from straight-line elements along constant percent chord lines. In this case the lines of discontinuity were streamwise.

The area distributions of the various models are shown in figure 3. Note that indenting the bodies eliminated most of the difference between models with the basic wing and the thickened modification. The area distribution of the blunted model was essentially equal to that shown for the basic model with the Sears-Haack body.

WIND TUNNEL AND CORRECTIONS

The present experimental investigation was conducted in the Ames 6- by 6-foot supersonic wind tunnel which is a closed-circuit variable-pressure type with a Mach number range continuous from 0.60 to 2.22. Recent modifications involved perforating the test-section floor and ceiling and adding a boundary-layer removal system to maintain uniform flow at transonic and low supersonic speeds. In addition, injector flaps were installed downstream of the test section to extend the upper Mach number limit by reducing the required compression ratio across the nozzle and by better matching the weight flow characteristics of the nozzle with those of the compressor.

Surveys of the stream characteristics in the region of the test section have shown that essentially no stream curvature exists in the pitch plane of the models and that axial static-pressure variations were usually less than ±1 percent of the dynamic pressure. This static-pressure variation resulted in negligible longitudinal-buoyancy corrections to the drag of these models. Therefore, no corrections were made for stream curvature or static-pressure variation in the present investigation.

From tests of the basic configuration in the normal and inverted attitudes, a stream angle, which was equal to or less than $\pm 0.40^\circ$ throughout the Mach number range, was found to exist in the pitch plane. The data presented herein have been corrected for these stream angles.

The effects of model support interference on the aerodynamic characteristics were considered to consist primarily of a change in the pressure at the base of the models. As a result, the base pressure was measured and corrected to free-stream static pressure and the drag data were then adjusted accordingly. Typical base-drag coefficients are listed in table III for the blunted model.

TESTS AND PROCEDURE

Force and moment data were obtained at Mach numbers of 0.65, 0.80, 0.90, 1.00, 1.10, 1.20, 1.40, 1.70, and 1.90 for angles of attack from -4° to a maximum of $\pm 18^\circ$. In addition, drag data at zero lift were obtained at Mach numbers of 0.70, 0.85, 0.95, 1.05, 1.15, 1.30, 1.50, 2.00, and 2.20. The test Reynolds number based on the basic-wing mean aerodynamic chord was 2.58 million at all Mach numbers.

Since most wind tunnels operate at relatively low Reynolds numbers, extensive regions of laminar flow can exist on the models at zero lift. The extent of this laminar flow can vary with Mach number and with wing leading-edge shape. For instance, the thickened or blunted sections could have less laminar flow than the basic section. Also, as the angle of attack is increased the transition point on the wing usually moves forward, thereby causing a change in friction drag which is difficult to evaluate and not necessarily representative of full scale. In order to induce transition at fixed locations on the wings and body, 0.005-inch-diameter grit was sprayed on the forward 15-percent chord of the wings from the wing-body juncture to the tip (both top and bottom surfaces) and on the nose of the bodies covering approximately one inch from the tip. The grit distribution was approximately 400 grains per square inch. To insure that transition was taking place, preliminary runs were made, both with and without fixed transition, utilizing the flow visualization techniques discussed in reference 5.

All aerodynamic coefficients are based on the complete plan-form area of the basic wing. The pitching-moment coefficients were computed about the quarter-chord position of the mean aerodynamic chord of the wing. Theoretical calculations of the wave drag were made by the method of reference 6, and the area distributions required for these calculations were made with electronic computing machines using procedures given in an appendix of reference 2. Prediction of laminar and turbulent friction drag without heat transfer at $M = 0$ was made by the method of reference 7. The variation of friction-drag coefficients with Mach number was computed

from the following equations:

Laminar flow, reference 8

$$\frac{C_{D_f}\sqrt{R}}{\left(C_{D_f}\sqrt{R}\right)_{M=0}} = \left(1 + 0.6\,\frac{\gamma-1}{2}\,M^2\right)^{-0.12}$$

Turbulent flow (smooth surface), reference 9

$$\frac{C_{D_f}}{\left(C_{D_f}\right)_{M=0}} = \left(1 + \frac{\gamma-1}{2}\,M^2\right)^{-0.467}$$

Turbulent flow (rough surface), reference 10

$$\frac{C_{D_f}}{\left(C_{D_f}\right)_{M=0}} = \left(1 + r\,\frac{\gamma-1}{2}\,M^2\right)^{-1}$$

where

$$r = 0.86$$

$$\gamma = 1.4$$

This last equation is required for the wing area covered by grit used to fix boundary-layer transition.

All the data presented under Results and Discussion will be with transition fixed. An illustration of the effect on the zero-lift drag coefficients of fixing transition with distributed roughness (as represented by the model with the basic wing and the Sears-Haack body) is shown in figure 4. The friction-drag coefficients attributed to fixing transition shown in figure 4(b) indicate that the grit produced no wave drag because the computed increments (relative to subsonic values) were actually

greater than the experimental increments at the highest Mach numbers.
For tests of wings with similar leading edges the grit could be confined
to a small region rearward of the leading edge and thus the grit would
cause a smaller drag-coefficient increment than that obtained for the
present investigation.

RESULTS AND DISCUSSION

The fundamental aerodynamic data for the basic and thickened leading-
edge wings with the Sears-Haack and indented bodies are presented in the
various parts of figure 5. As in prior investigations, the thickened
modification primarily affected the drag data and resulted generally in
lower drag at high lift and subsonic Mach numbers (figs. 5(c) and 5(f)).
However, even with indented bodies the drag of the thickened model was
greater than that of the basic model at the higher supersonic Mach
numbers (fig. 5(f)).

Data for the blunted model were taken at only a few Mach numbers
and the results are listed in table III. The lift and pitching-moment
data are quite similar to those for the basic model; however, at high
angles of attack and subsonic Mach numbers the blunted model did not have
the lower drag characteristics typical of the thickened leading-edge
configurations discussed in reference 3. It is believed that the lack
of subsonic improvement is due to the changes in curvature on the upper
surface of the wing as shown in figure 2. These changes existed because
the design was intended to simulate only the thickness distribution of a
slightly cambered design which would have been free of any erratic
curvature on the upper surface.

The zero-lift drag coefficients of the various models are shown in
figure 6. The dip in these data at Mach numbers from 1.10 to 1.20 is
probably due to the reflected bow wave impinging on the model. The
increase in zero-lift drag coefficients of the thickened and blunted
models over those for the basic models is shown in figure 7. Figures 6
and 7 illustrate that even though the indentations reduced the drag at
all Mach numbers, and removed the small drag differences at transonic
speeds, the penalty for the thickened modification at speeds near and
above sonic-leading-edge conditions was not removed $(M \geq \sqrt{2},$
$(\Delta C_{D_O})_{mod} = 0.0040$ to $0.0060)$. The increased volume near the wing tip
of the thickened wing results in a large variation in the equivalent area
curves with Mach number, such that an average contoured body is only
partially effective in reducing the wave drag at the higher Mach numbers.
The drag penalty due to the blunted modification was generally less than
one quarter the value for the thickened modification. This illustrates
that much of the drag penalty is due to the increased wing volume and
some of the drag penalty is due purely to bluntness of the wing.

The effect of the wing sections and the bodies on the maximum
lift-drag ratio for the various models is shown in figure 8. As mentioned
previously, it is again apparent that the model with the blunt section,
as tested, has no performance advantage at high subsonic speeds.

The effects of the indentations in reducing the wave-drag coefficients
at transonic speeds and the smaller effects at higher speeds were indicated
by theoretical calculations as well as by experiment as shown in figures 9
and 10. In the computations for the variation in friction-drag coeffi-
cients with Mach number (in order to determine the experimental wave-drag
coefficients) the friction drag for turbulent flow over a smooth surface
was increased slightly to match the experimental results at $M = 0.65$.
It is of interest to note that the indentations were successful in reducing
the wave-drag coefficients at all test and design Mach numbers, even
though the linear theory used is not intended to apply for Mach numbers
equal to or greater than sonic-leading-edge conditions. Figures 9 and 10
illustrate that for blunt leading-edge wings (even the basic wing is
considered to be blunt or not sharp) the theory becomes progressively
worse as the bluntness is increased and that the theoretical calculations
may not always be conservative or indicate trends for these wings (for
supersonic-leading-edge conditions).

CONCLUDING REMARKS

The increased volume and bluntness of the model with the thickened
leading-edge modification resulted in an increase in zero-lift drag
coefficient of 0.0040 to 0.0060 over values for the basic model at Mach
numbers at which the wing leading edge was sonic or supersonic. Although
the drag coefficients of both the basic and thickened models were reduced
at all test Mach numbers by body indentations designed for the range of
Mach numbers from 1.00 to 2.00, the greater drag of the thickened model
relative to the basic model was not reduced. The blunted model, however,
with wing volume comparable to the basic model had less than one quarter
of the drag penalty of the thickened model relative to the basic model
at supersonic-leading-edge conditions ($M \geq \sqrt{2}$).

Ames Research Center
    National Aeronautics and Space Administration
        Moffett Field, Calif., March 20, 1959

REFERENCES

1. Graham, David, and Evans, William T.: Investigation of the Effects of an Airfoil Section Modification on the Aerodynamic Characteristics at Subsonic and Supersonic Speed of a Thin Swept Wing of Aspect Ratio 3 in Combination With a Body. NACA RM A55D11, 1955.

2. Holdaway, George H., and Hatfield, Elaine W.: Investigation of Symmetrical Body Indentations Designed to Reduce the Transonic Zero-Lift Wave Drag of a 45° Swept Wing With an NACA 64A006 Section and With a Thickened Leading-Edge Section. NACA RM A56K26, 1957.

3. Evans, William T.: Leading-Edge Contours for Thin Swept Wings: An Analysis of Low- and High-Speed Data. NACA RM A57B11, 1957.

4. Lomax, Harvard, and Heaslet, Max. A.: Recent Developments in the Theory of Wing-Body Wave Drag. Jour. Aero. Sci., vol. 23, no. 12, Dec. 1956, pp. 1061-1074.

5. Main-Smith, J. D.: Chemical Solids as Diffusible Coating Films for Visual Indication of Boundary-Layer Transition in Air and Water. British R.&M. No. 2755, Feb. 1950.

6. Holdaway, George H., and Mersman, William A.: Application of Tchebichef Form of Harmonic Analysis to the Calculation of Zero-Lift Wave Drag of Wing-Body-Tail Combinations. NACA RM A55J28, 1956.

7. Hall, Charles F., and Fitzgerald, Fred F.: An Approximate Method for Calculating the Effect of Surface Roughness on the Drag of an Airplane. NACA RM A7B24, 1947.

8. Rubesin, M. W., and Johnson, H. A.: A Critical Review of Skin Friction and Heat Transfer Solutions of the Laminar Boundary Layer of a Flat Plate. Trans. ASME, vol. 71, no. 4, May 1, 1949, pp. 383-388.

9. Rubesin, Morris W., Maydew, Randall C., and Varga, Steven A.: An Analytical and Experimental Investigation of the Skin Friction of the Turbulent Boundary Layer on a Flat Plate at Supersonic Speeds. NACA TN 2305, 1951.

10. Goddard, Frank E., Jr.: Effect of Uniformly Distributed Roughness on Turbulent Skin-Friction Drag at Supersonic Speeds. Jour. Aero./Space Sci., vol. 26, no. 1, Jan. 1959.

TABLE I.- BODY COORDINATES IN INCHES

Sears-Haack body		Indented[1] body for basic wing		Indented[1] body for thickened wing	
Station	Radius	Station	Radius	Station	Radius
0	0	0	0	0	0
.595	.210	.595	.210	1.058	.327
1.190	.353	1.190	.353	2.116	.542
2.380	.583	2.380	.583	3.173	.716
3.570	.777	3.570	.777	4.231	.878
4.760	.951	4.760	.951	5.289	1.023
5.950	1.107	5.950	1.107	6.347	1.160
7.140	1.248	7.140	1.246	7.404	1.277
8.330	1.375	8.330	1.372	8.462	1.388
9.520	1.494	9.520	1.491	9.520	1.493
10.710	1.603	10.710	1.598	10.578	1.589
11.900	1.703	11.900	1.694	11.636	1.675
13.090	1.795	13.090	1.780	12.693	1.753
14.280	1.879	14.280	1.856	13.751	1.824
15.470	1.955	15.470	1.921	14.809	1.886
16.660	2.025	16.660	1.969	15.867	1.939
17.850	2.089	17.850	1.996	16.924	1.976
19.040	2.145	19.040	2.008	17.982	1.993
20.230	2.195	20.230	2.009	19.040	1.997
21.420	2.239	21.420	2.001	20.098	1.980
22.610	2.277	22.610	1.985	21.156	1.965
23.800	2.308	23.800	1.961	22.213	1.936
24.990	2.334	24.990	1.943	23.271	1.903
26.180	2.354	26.180	1.935	24.329	1.880
27.370	2.369	27.370	1.936	25.387	1.864
28.560	2.377	28.560	1.942	26.444	1.857
29.750	2.380	29.750	1.961	27.502	1.857
30.940	2.377	30.940	1.992	28.560	1.874
32.130	2.368	32.130	2.016	29.618	1.896
33.320	2.354	33.320	2.037	30.676	1.923
34.510	2.334	34.510	2.050	31.733	1.952
35.700	2.308	35.700	2.064	32.791	1.988
36.890	2.277	36.890	2.068	33.849	2.011
38.080	2.239	38.080	2.064	34.907	2.032
39.270	2.195	39.270	2.045	35.964	2.044
40.460	2.145	40.460	2.016	37.022	2.048
41.650	2.089	41.650	1.974	38.080	2.046
42.840	2.025	42.840	1.926	39.138	2.034
44.030	1.955	44.030	1.867	40.196	2.010
45.220	1.879	45.220	1.801	41.253	1.977
46.410	1.795	46.410	1.728	42.311	1.936
46.933	1.754	46.933	1.691	43.369	1.893
				44.427	1.840
				45.484	1.780
				46.542	1.715
				46.933	1.683

[1]Indentation averaged for M = 1.00 to 2.00.

TABLE II.- COORDINATES OF THE AIRFOIL SECTIONS
(a) Basic and thickened
[Sections normal to 39.45° sweep line]

100 x'/c'	Basic section	Thickened sections		
	$\eta=$ 0 to 1.00	$\eta=0$	$\eta=0$ to 0.55	$\eta=$ 0.55 to 1.00
	100 t/2c'	100 t/2c'	100 t/2c'	100 t/2c'
0	0	0	Straight line fairing from $\eta=0$ to $\eta=0.55$ along constant percent chord lines	0
.50	.485	.696		.891
.75	.585	.840		1.075
1.25	.739	1.058		1.354
2.50	1.016	1.430		1.818
5.00	1.399	1.891		2.355
7.50	1.684	2.188		2.659
10	1.919	2.393		2.836
15	2.283	2.641		2.981
20	2.557	2.790		3.000
25	2.757	2.883		3.000
30	2.896	2.949		3.000
35	2.977	2.986		3.000
40	2.999	2.999		2.999
45	2.945	(1)	(1)	(1)
50	2.825			
55	2.653			
60	2.438			
65	2.188			
70	1.907			
75	1.602			
80	1.285			
85	.967			
90	.649			
95	.331			
100	.013			
Leading-edge radius, percent c'	0.246	0.534		0.90

[1]Same as the basic section (NACA 64A006).

TABLE II.- COORDINATES OF THE AIRFOIL SECTIONS - Concluded

(b) Basic and blunted

[Sections streamwise]

100 x/c	Basic section η=0 to 100	Blunted sections		
		η= 0 to 0.40	η= 0.40 to 0.60	η= 0.60 to 1.00
	100 t/2c	100 t/2c	100 t/2c	100 t/2c
0	0			
.67	.464			
1.01	.559			
1.34	---	0	Straight line	0
1.68	.705	.335	fairing from	.628
2.02	---	.489	η=0.40 to	.852
2.68	---	.716	η=0.60 along	1.096
3.34	.965	.884	constant per-	1.223
4.00	---	1.010	cent chord	1.276
4.66	---	1.108	lines	1.285
5.32	---	1.181		1.269
5.97	---	1.252		1.272
6.62	1.317	1.317		1.317
9.85	1.571	(1)	(1)	(1)
13.02	1.775			
19.21	2.077			
25.20	2.289			
31.00	2.428			
36.61	2.511			
42.05	2.541			
47.32	2.520			
52.44	2.438			
57.41	2.302			
62.22	2.132			
66.90	1.931			
71.45	1.709			
75.87	1.468			
80.17	1.216			
84.35	.963			
88.42	.715			
92.38	.474			
96.24	.238			
100.00	.009			
Leading-edge radius, per-cent c	0.167	0.167		[2]0.612

[1]Same as the basic section.
[2]Same as for the thickened section.

TABLE III.- AERODYNAMIC DATA FOR THE MODEL WITH THE BLUNTED LEADING EDGE

M	α, deg	c_L	c_m	c_D	c_{D_b}	L/D
0.65	-1.13	-0.0670	0.0035	0.0120	0.0014	---
	-.09	-.0068	.0005	.0115	.0015	---
	.90	.0630	-.0038	.0117	.0014	5.38
	3.87	.2580	-.0116	.0202	.0017	12.76
	5.85	.3947	-.0193	.0364	.0017	10.84
	7.78	.5422	-.0306	.0665	.0019	8.16
0.90	-.96	-.0738	.0084	.0134	.0012	---
	.08	.0034	.0007	.0124	.0012	.27
	1.02	.0895	-.0069	.0133	.0013	6.73
	4.06	.3424	-.0369	.0305	.0016	11.20
	6.02	.5091	-.0701	.0613	.0013	8.30
	7.88	.6081	-.0747	.0923	.0019	6.59
1.40	-1.04	-.0601	.0133	.0236	.0040	---
	-.05	-.0036	.0010	.0226	.0040	---
	.94	.0584	-.0126	.0235	.0040	2.48
	3.96	.2347	-.0544	.0381	.0041	6.18
	5.98	.3500	-.0836	.0576	.0044	6.08
	7.87	.4567	-.1107	.0828	.0048	5.52
1.60	-1.08	-.0599	.0161	.0231	.0038	---
	-.09	-.0114	.0049	.0220	.0038	---
	.91	.0393	-.0064	.0226	.0037	1.74
	3.93	.1900	-.0415	.0351	.0039	5.42
	5.91	.2864	-.0654	.0513	.0042	5.58
	7.84	.3728	-.0858	.0720	.0046	5.18
1.90	-.76	-.0296	.0080	.0229	.0036	---
	.18	.0103	-.0016	.0225	.0035	.46
	1.12	.0518	-.0103	.0235	.0035	2.20
	4.14	.1791	-.0385	.0354	.0037	5.06
	6.17	.2628	-.0578	.0507	.0038	5.18
	8.09	.3544	-.0808	.0721	.0041	4.92

Aspect ratio = 3

Wing area = 351.31 sq in.

Taper ratio = 0.4

Dimensions in inches

Equation of body radii

$$\frac{r}{r_{max}} = \left[1 - \left(1 - \frac{x}{L/2}\right)^2 \right]^{3/4}$$
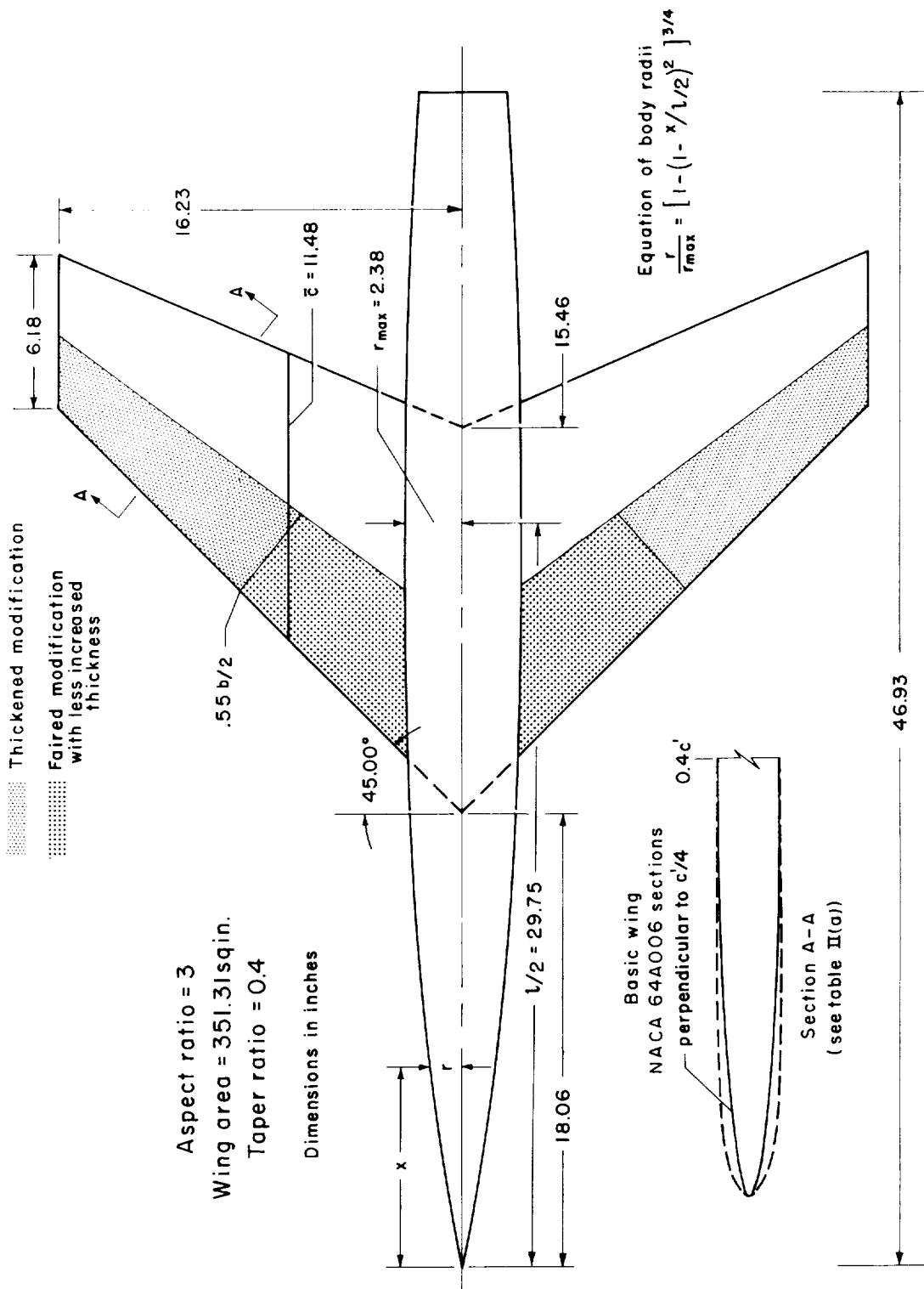
(a) Basic and thickened wings.

Figure 1.- Geometric details of the wings with the Sears-Haack body.

16

Aspect ratio = 3.04
Wing area = 346.60 sq in.
Taper ratio = 0.4

Dimensions in inches

16.23

6.10

$\bar{c}$ = 11.33

r_{max} = 2.38

.6 b/2

.4 b/2

44.77°

15.25

Equation of body radii

$$\frac{r}{r_{max}} = \left[1 - \left(1 - \frac{x}{l/2}\right)^2\right]^{3/4}$$

46.93

x

r

l/2 = 29.75

18.27

0.066c

Basic wing

Section A-A

Section B-B

(see table II(b))

A

A

B

B

Blunted modification

Faired modification

Shortened modification
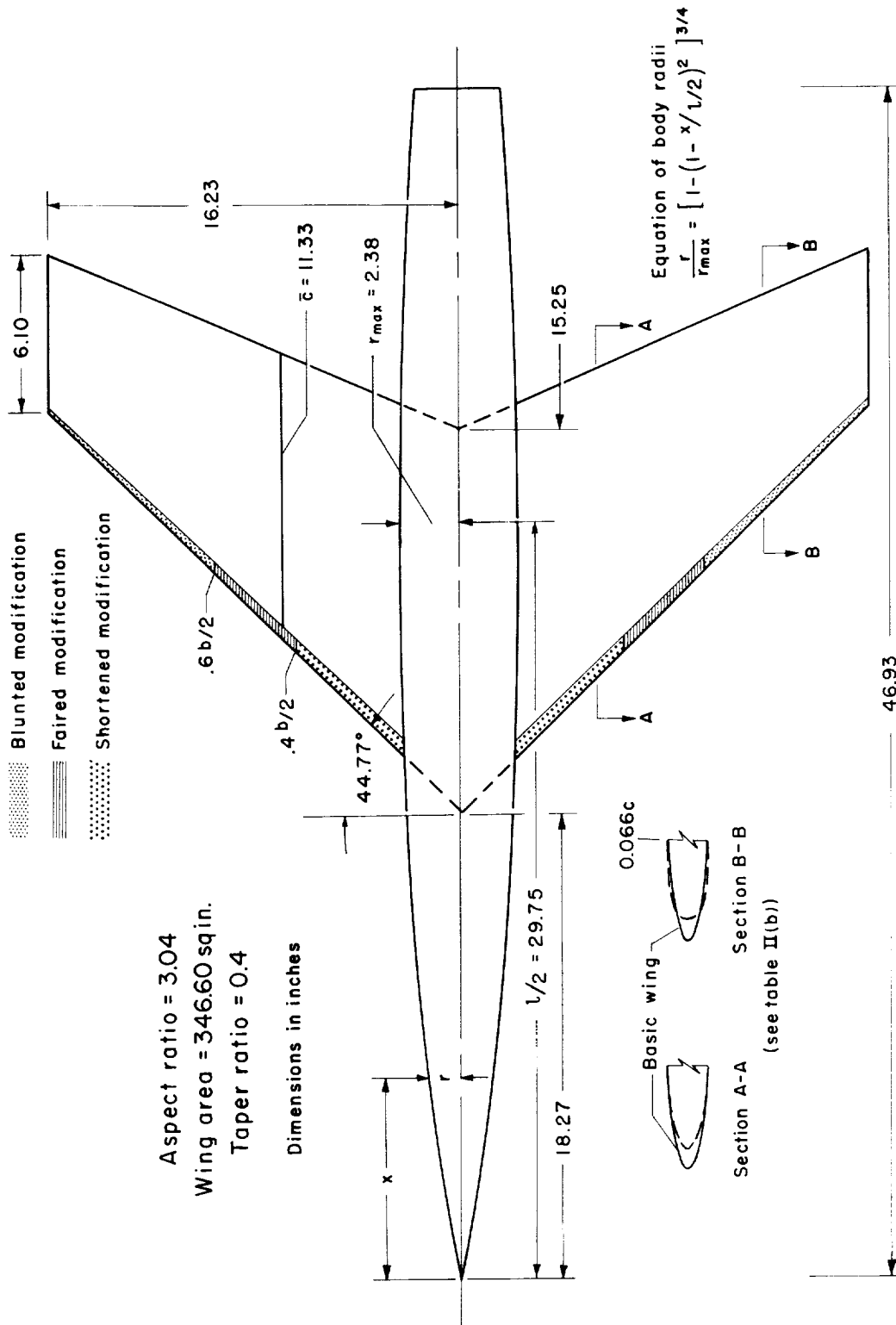
(b) Blunted wing.

Figure 1.- Concluded.
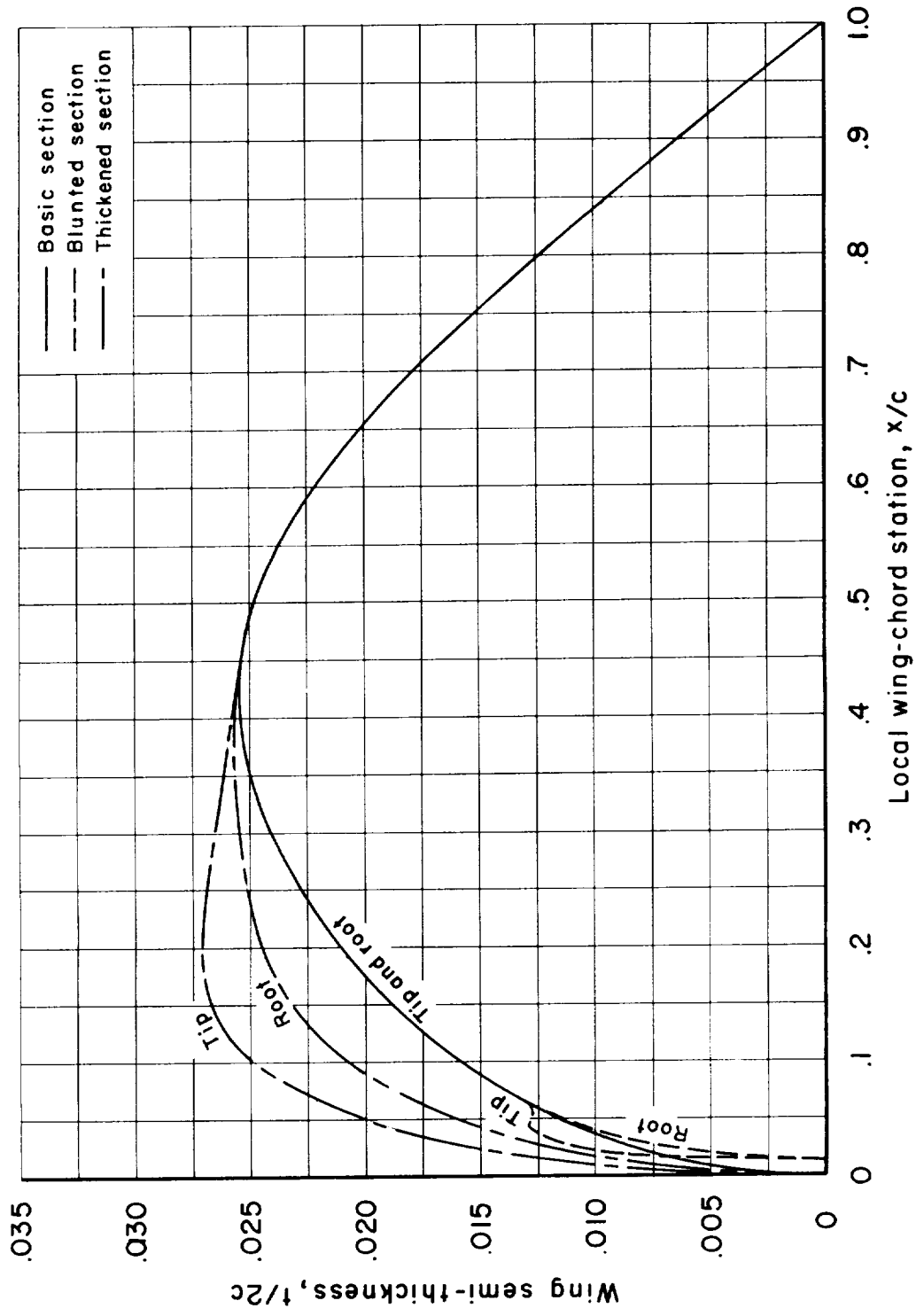
Figure 2.- Dimensionless streamwise sections of the three wings.
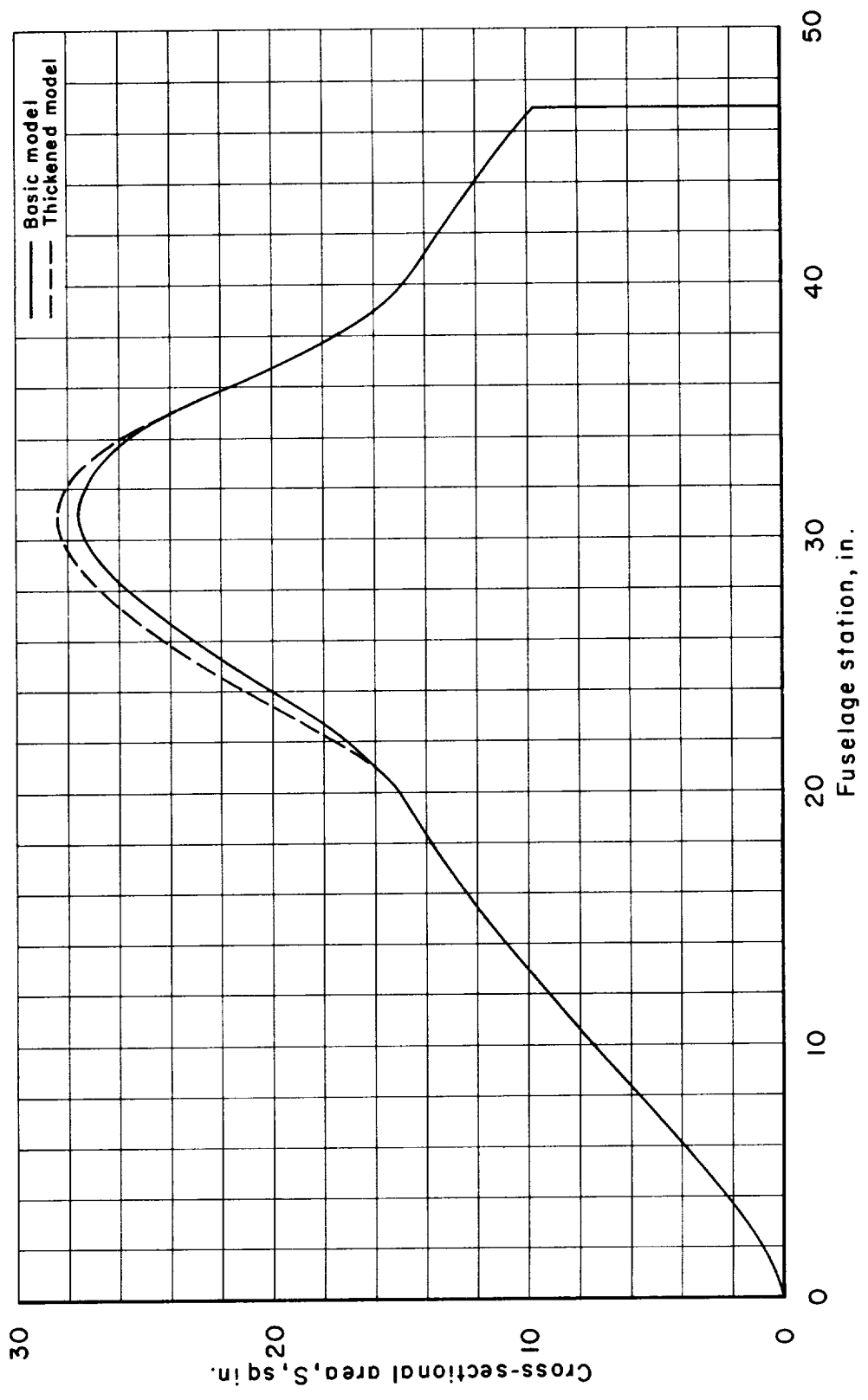
(a) Sears-Haack body.

Figure 3.- Cross-sectional area distributions of the basic and thickened wings with the various bodies.
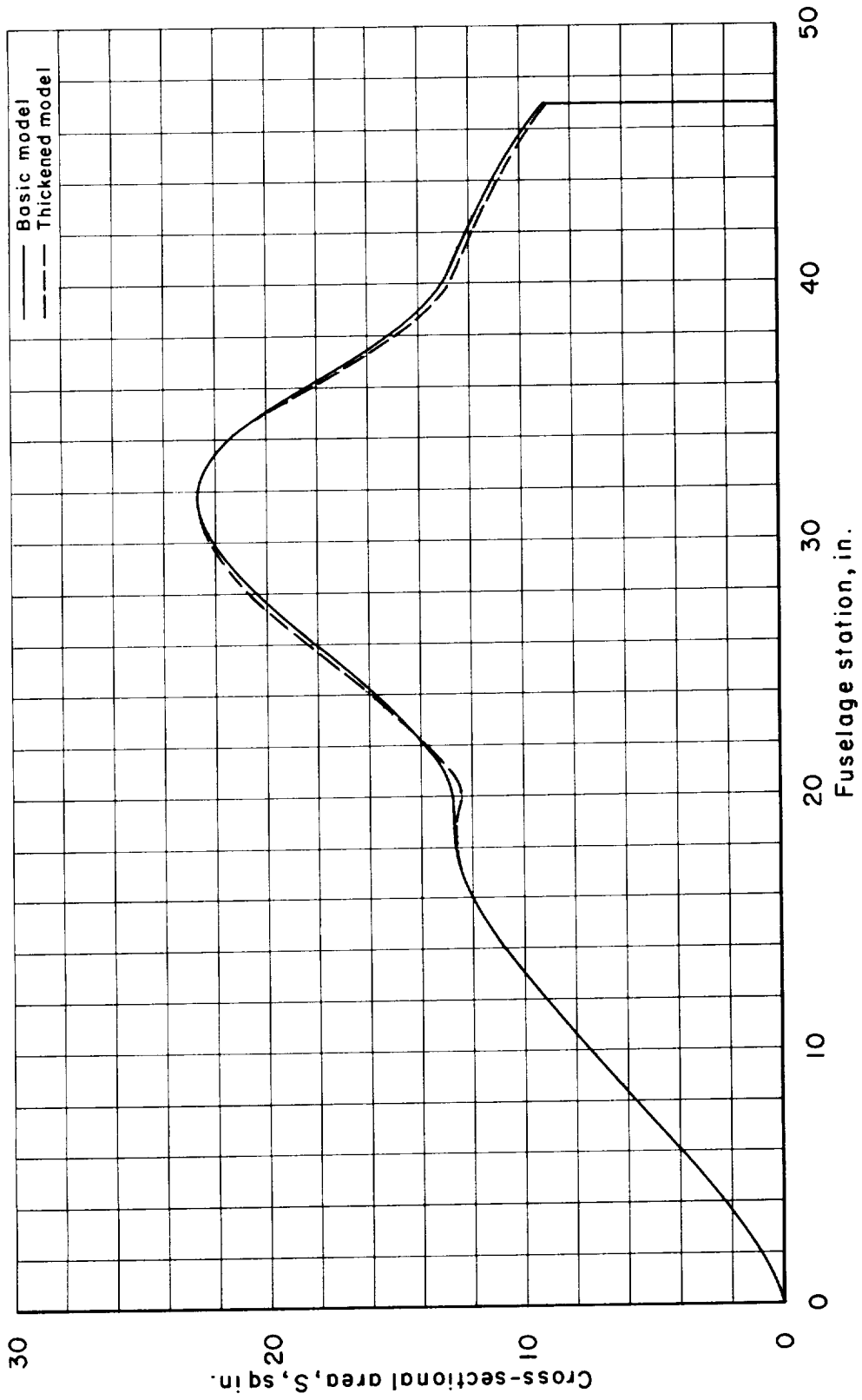
(b) M = 1.00 to 2.00 indented bodies.

Figure 3.- Concluded.

(a) Zero-lift drag coefficient.

(b) Zero-lift drag coefficient attributed to fixing transition.
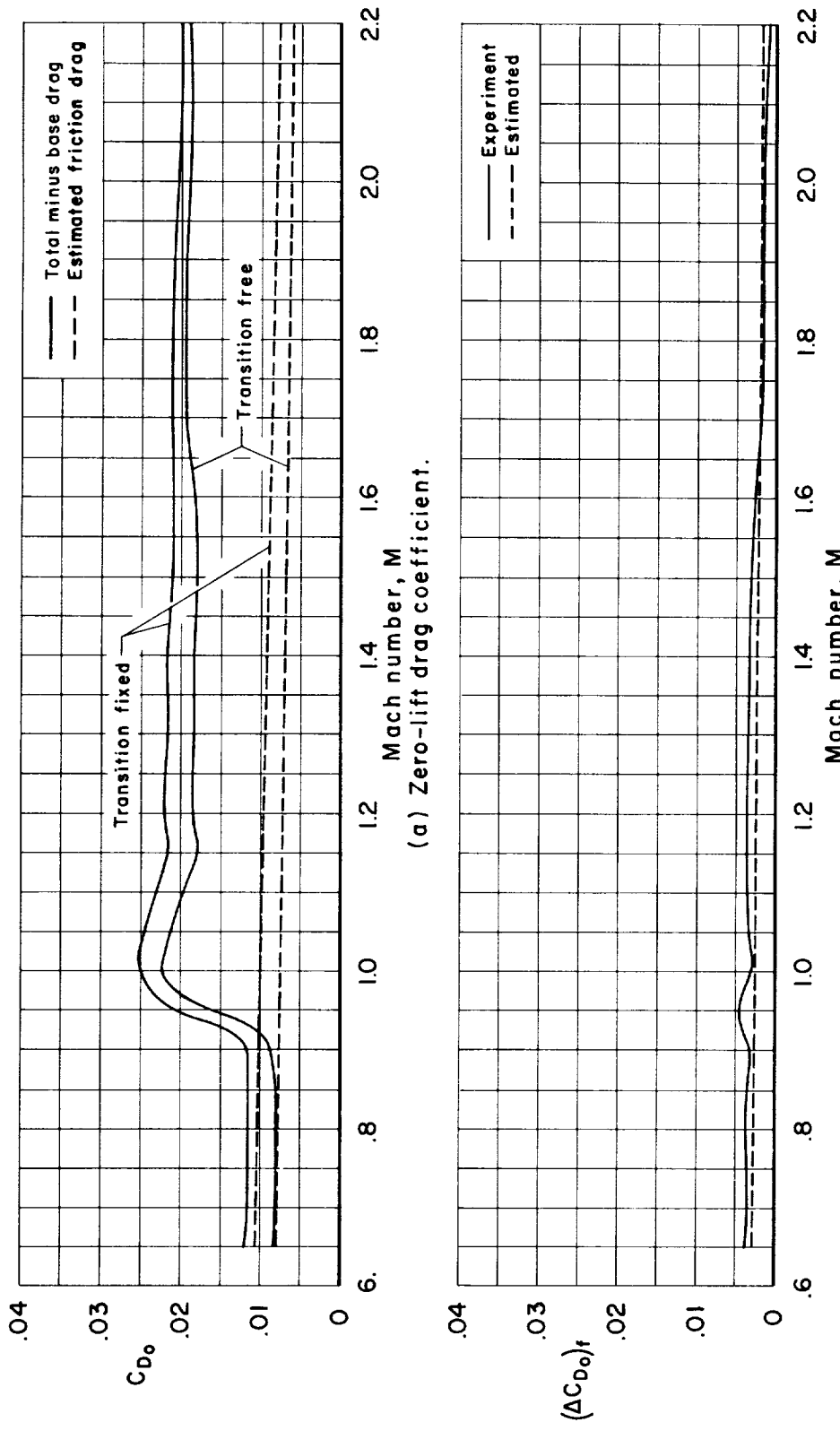
Figure 4.- Representative effect on zero-lift drag coefficient of fixing transition with distributed roughness; basic wing with the Sears-Haack body.
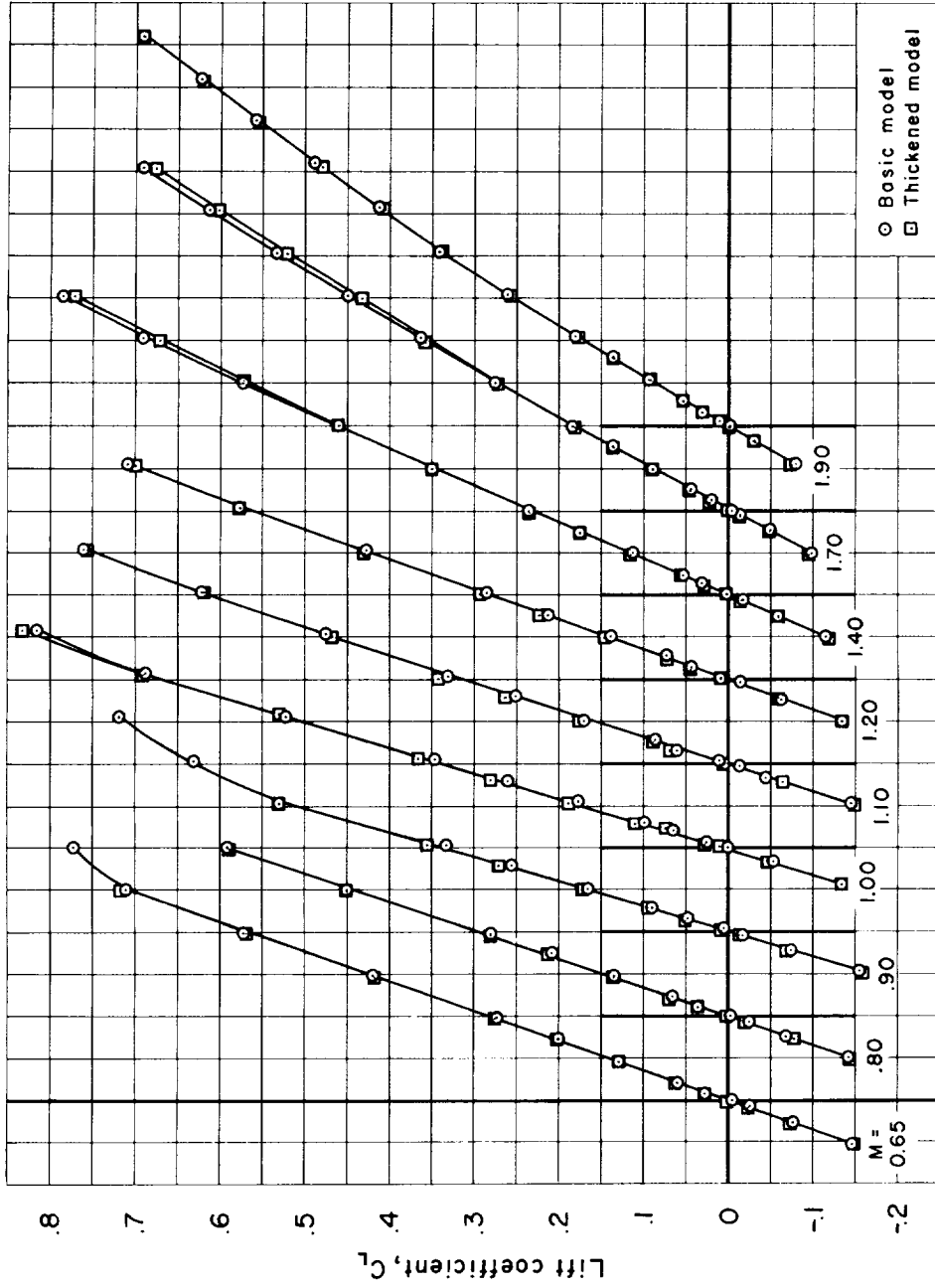
(a) C_L vs. α, Sears-Haack body.

Figure 5.- Aerodynamic characteristics with transition fixed of the basic and thickened models.

Pitching-moment coefficient, C_m
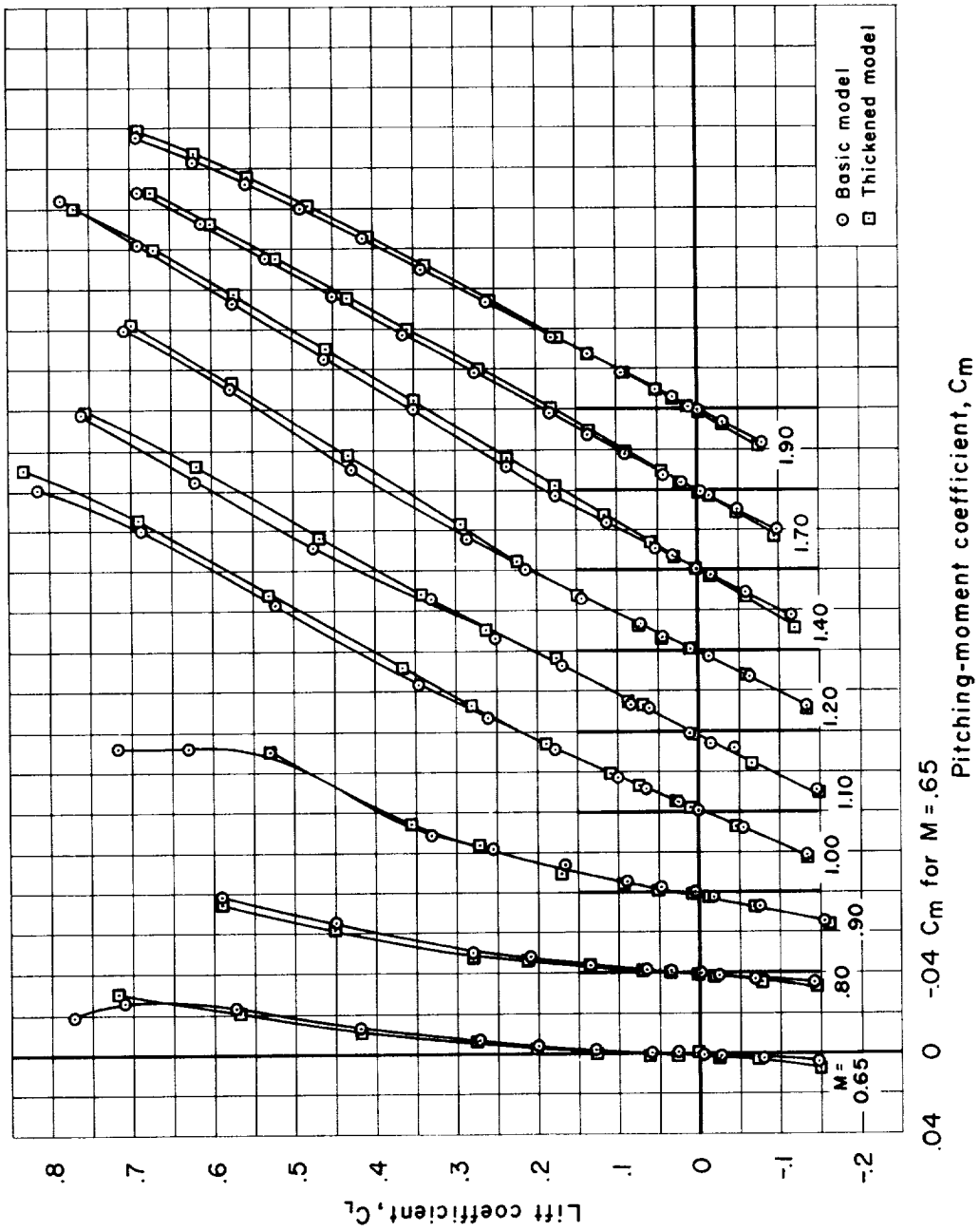
(b) C_L vs. C_m, Sears-Haack body.

Figure 5.- Continued.
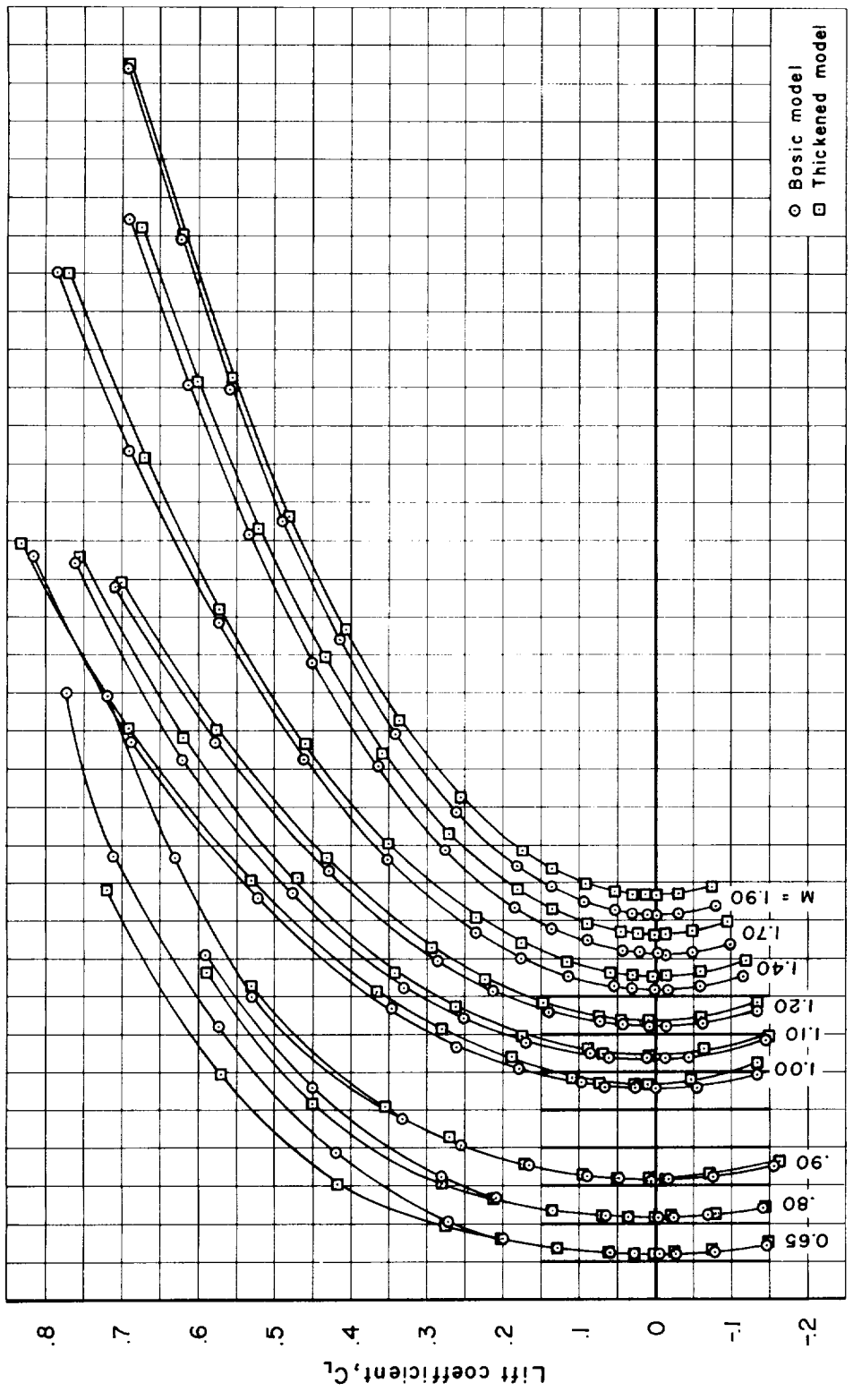
(c) C_L vs. C_D, Sears-Haack body.

Figure 5.- Continued.
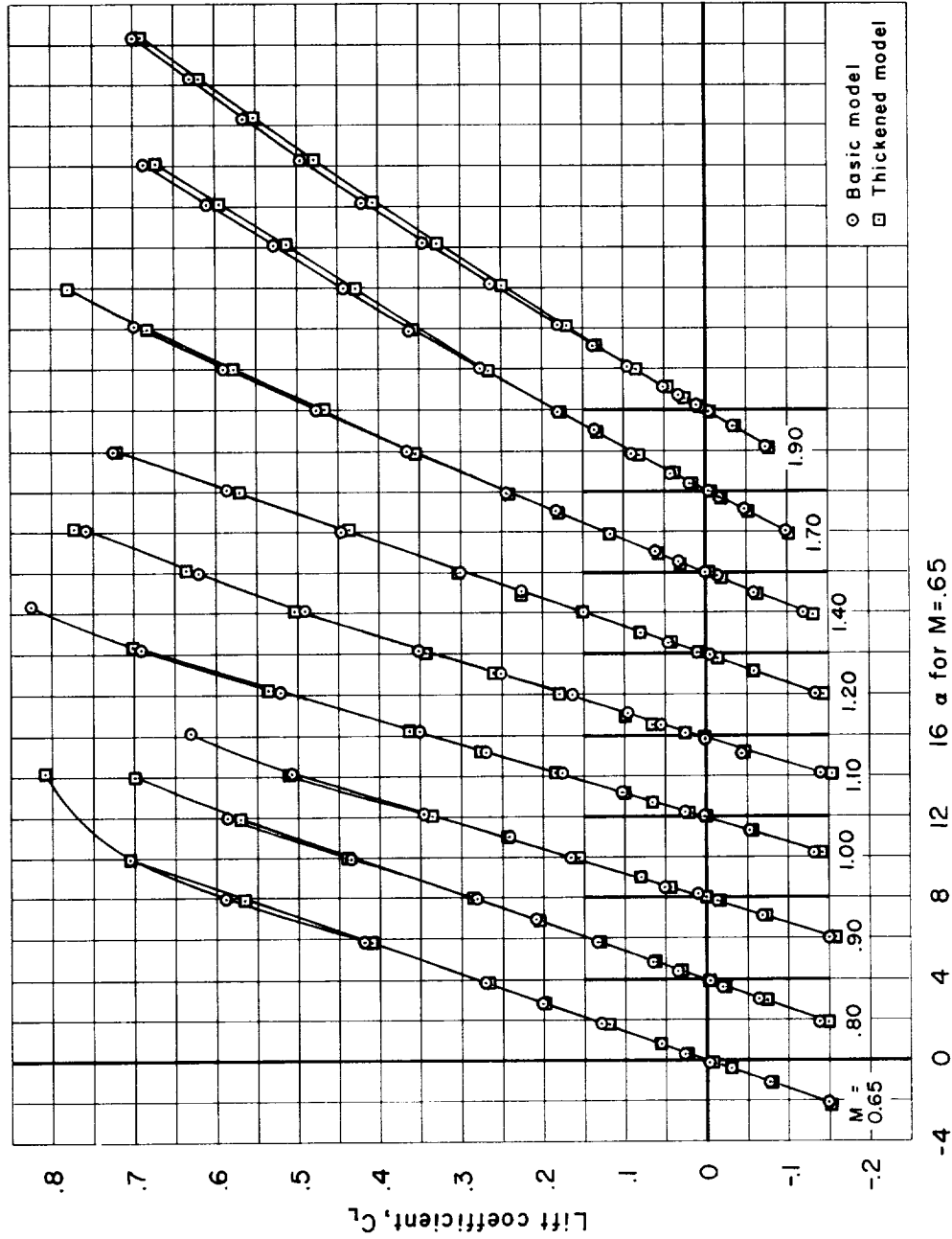
(d) C_L vs. α, M = 1.00 to 2.00 indented bodies.

Figure 5.- Continued.

Pitching-moment coefficient, C_m
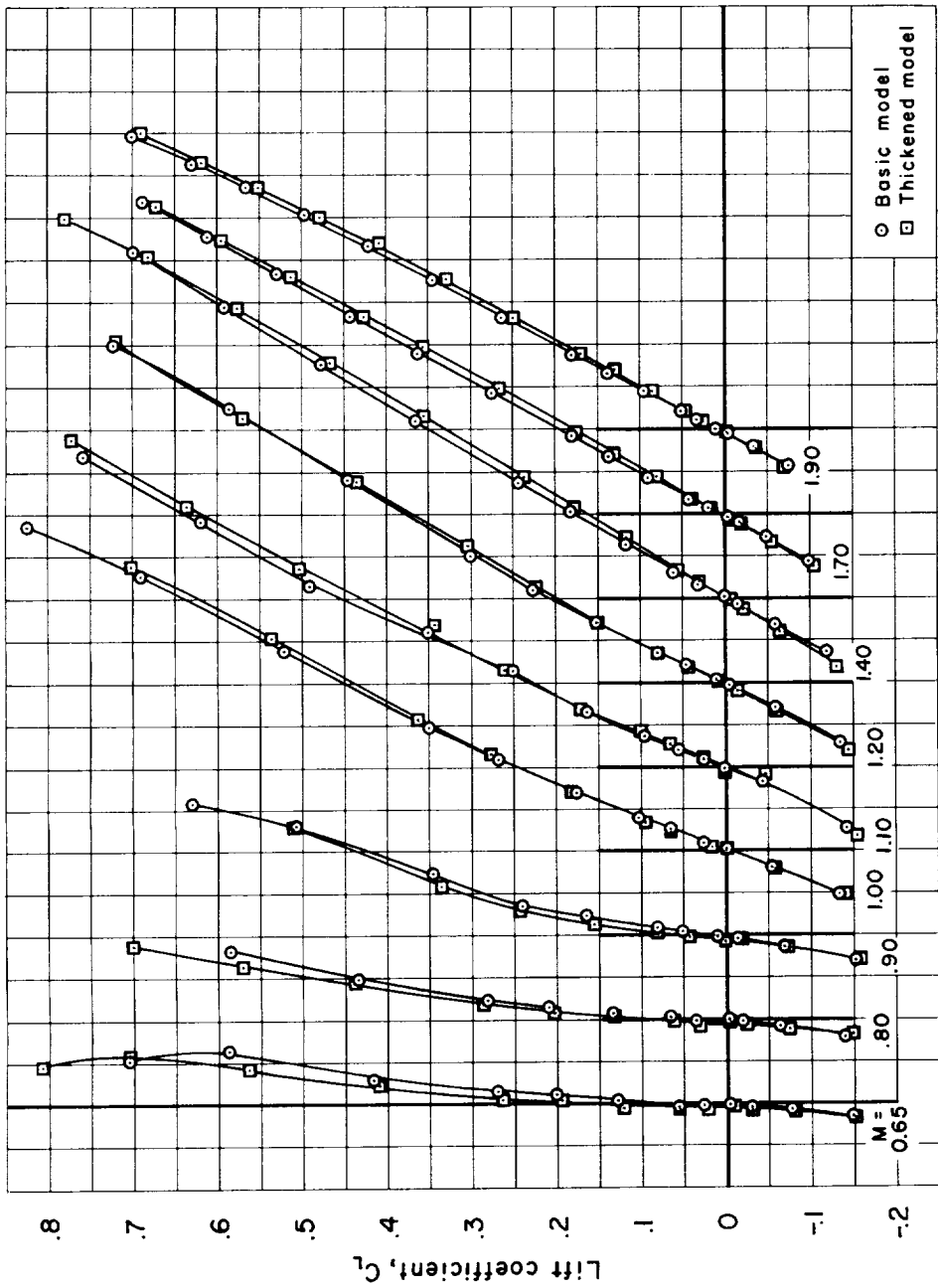
(e) C_L vs. C_m, M = 1.00 to 2.00 indented bodies.

Figure 5.- Continued.
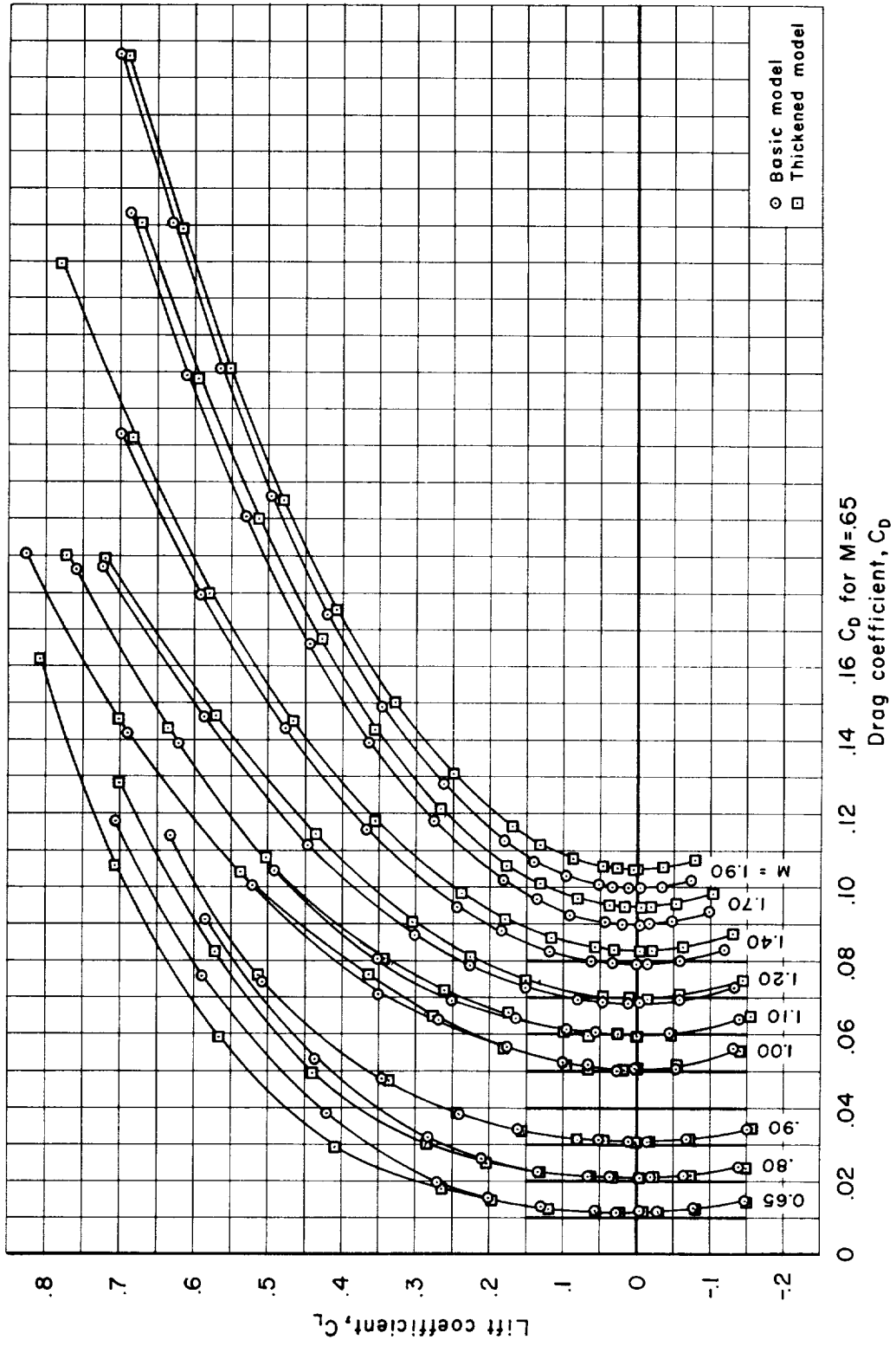
(f) C_L vs. C_D, M = 1.00 to 2.00 indented bodies.

Figure 5.- Concluded.
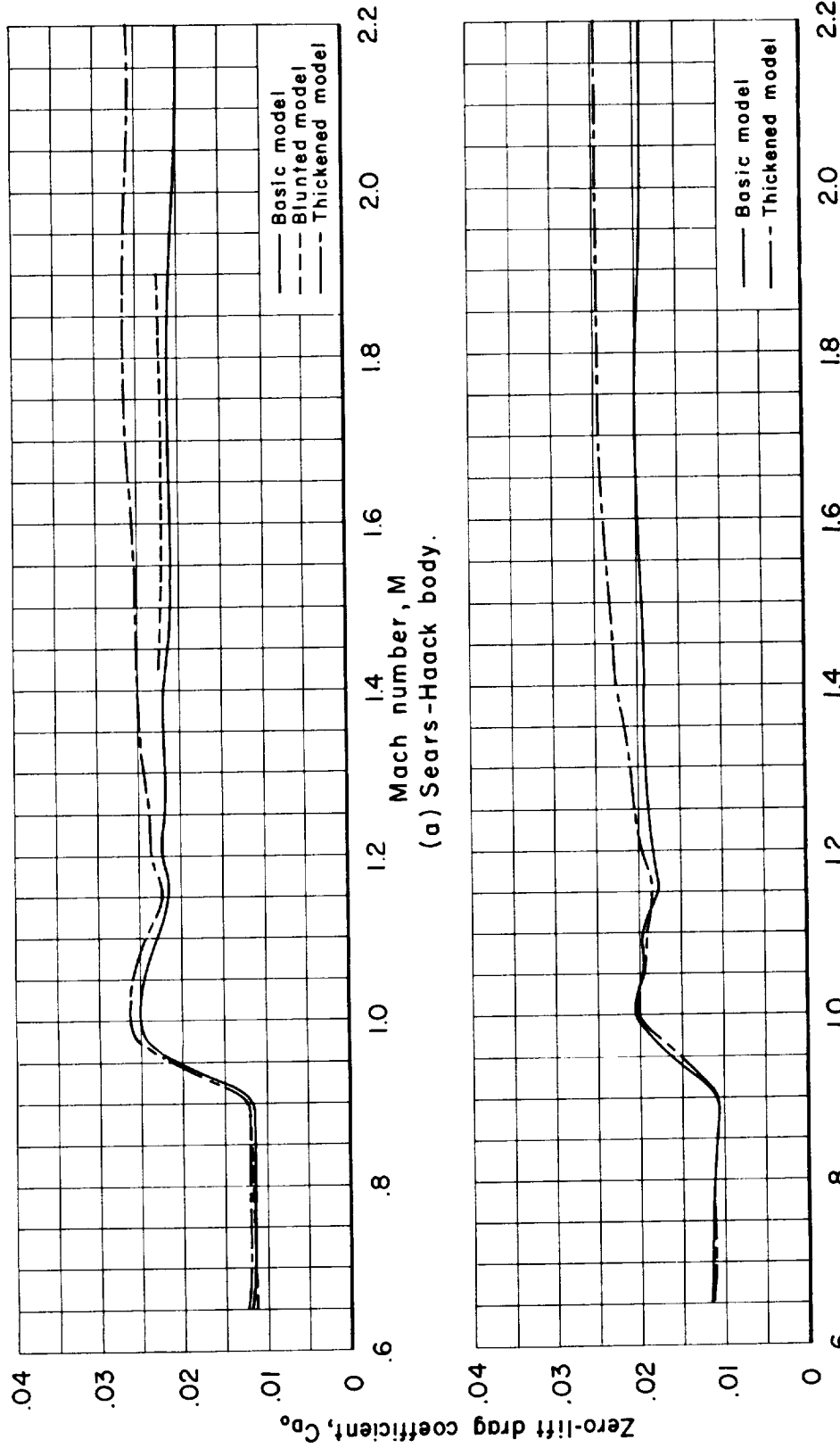
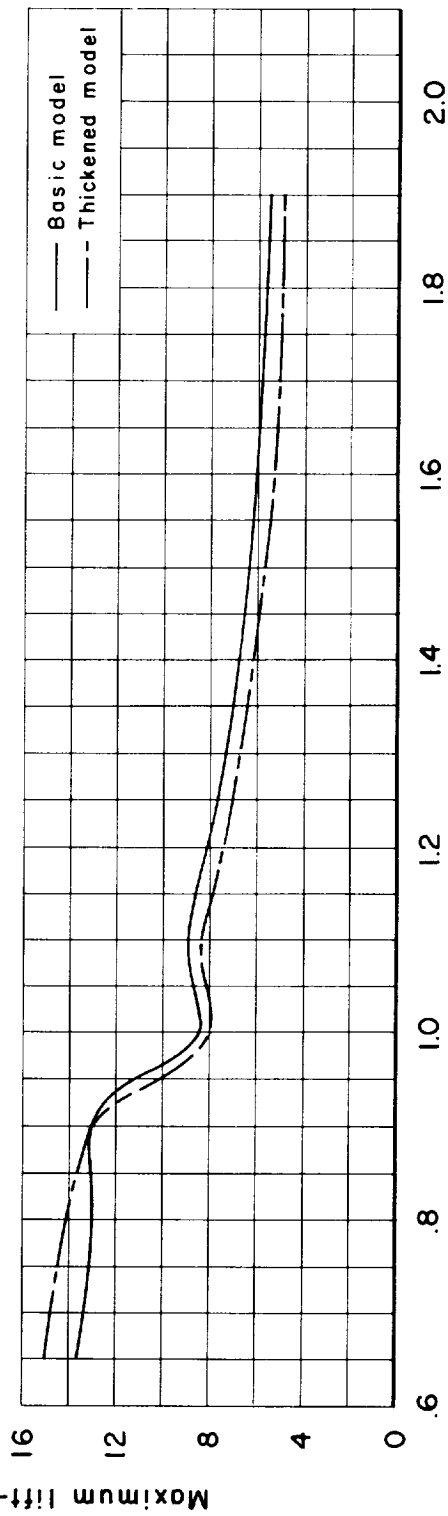Figure 6.- Zero-lift drag coefficients of the various models with transition fixed.

(a) Sears-Haack body.

(b) M=1.00 to 2.00 indented bodies.
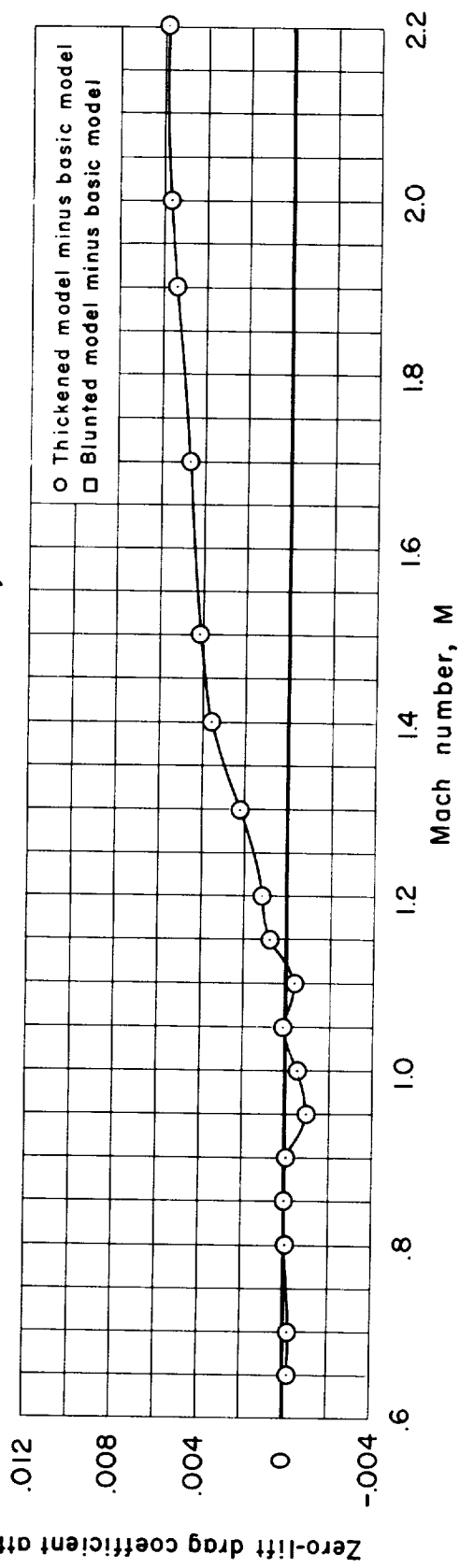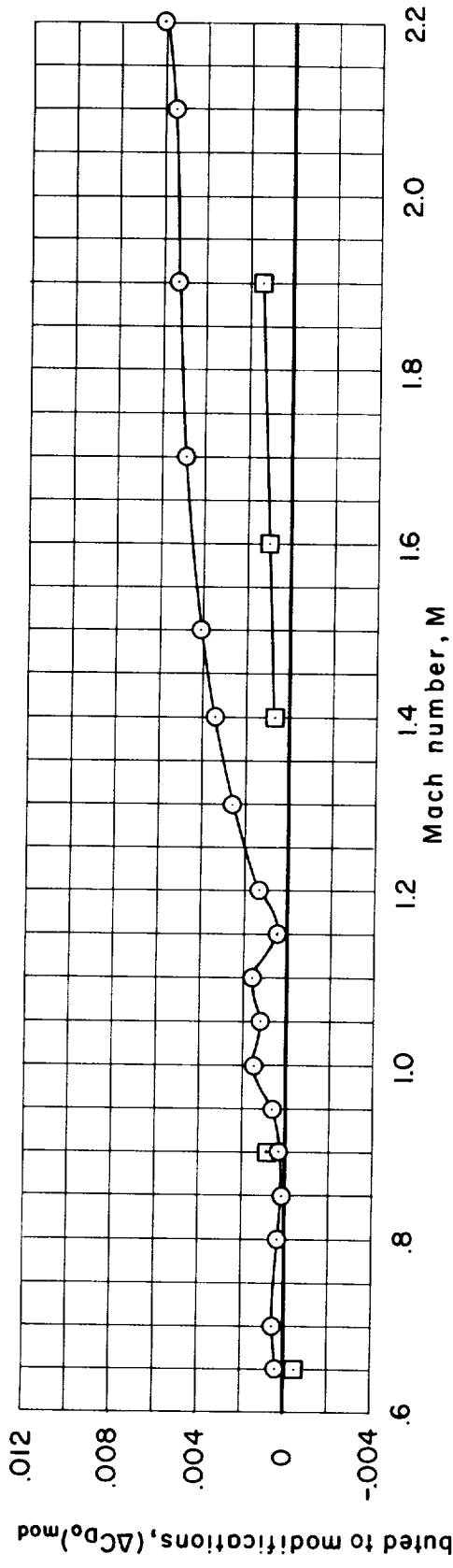
Figure 7.- Zero-lift drag coefficients attributed to the leading-edge modifications of the wing sections.

(a) Sears-Haack body.

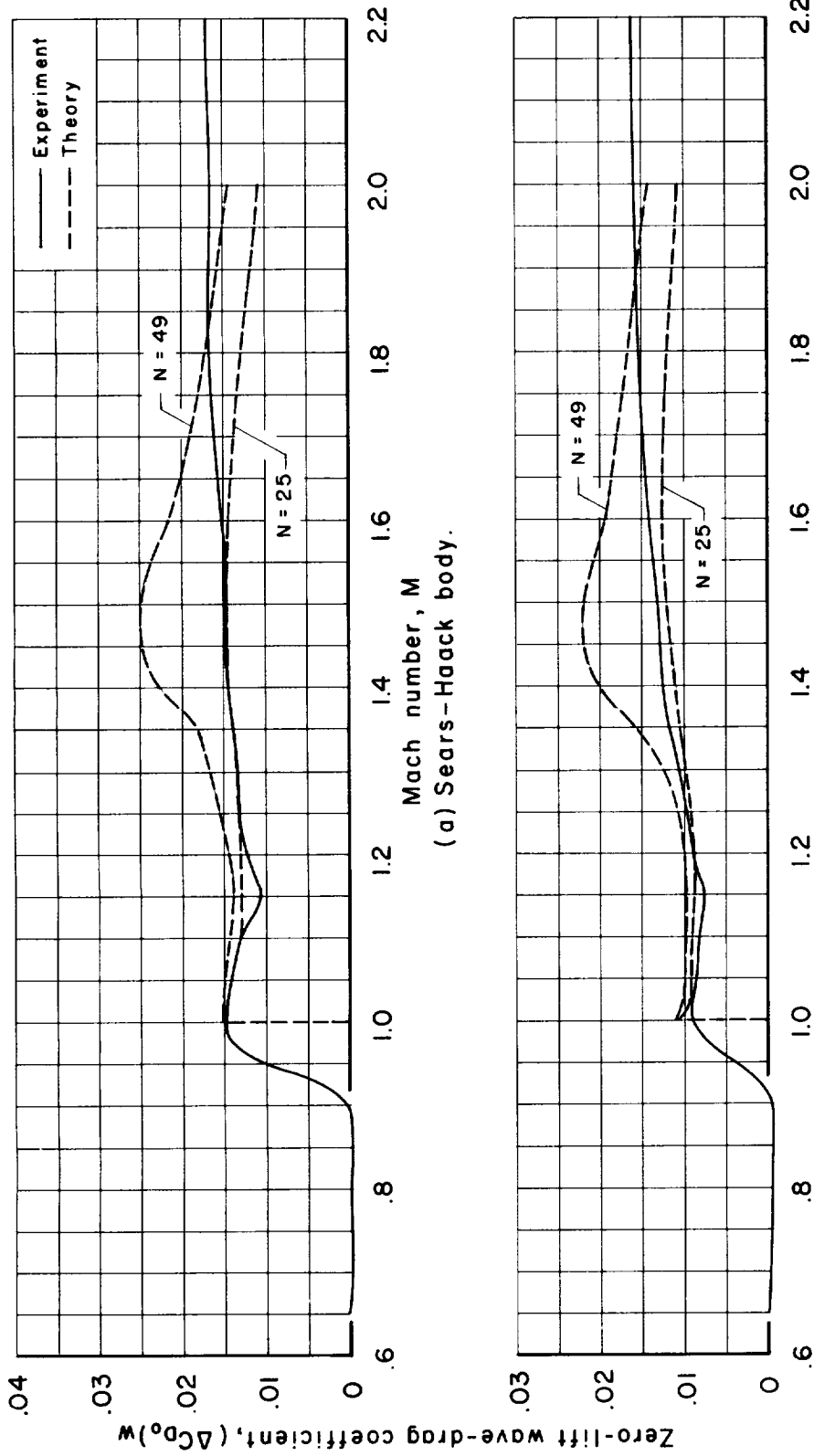(b) M=1.00 to 2.00 indented bodies.

Mach number, M

Zero-lift drag coefficient attributed to modifications, $(\Delta C_{D_0})_{mod}$

○ Thickened model minus basic model
□ Blunted model minus basic model
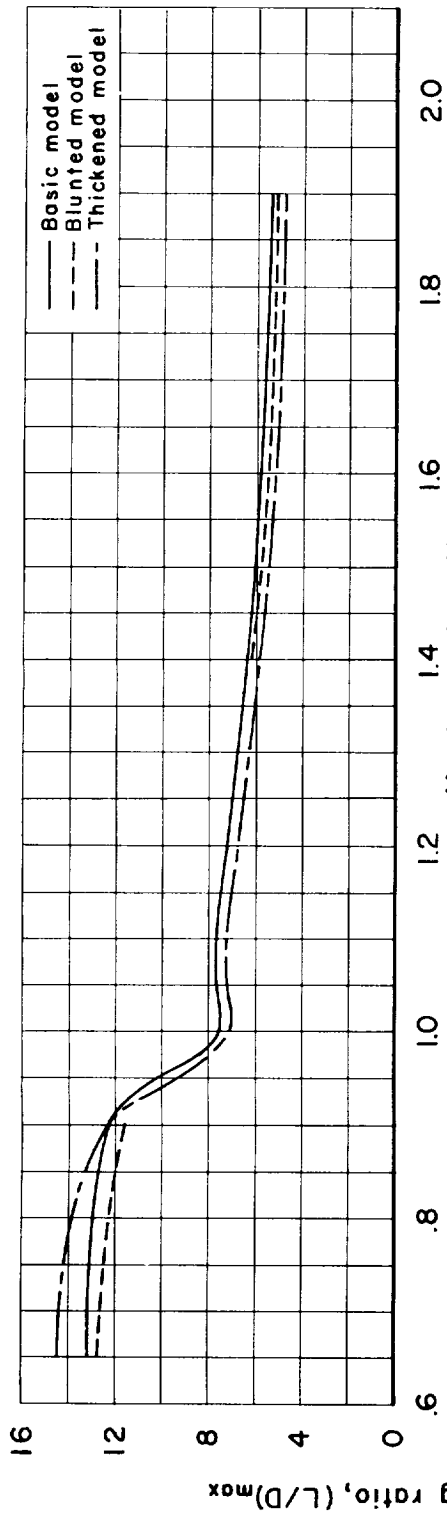
Figure 8.- Maximum lift-drag ratios of the various models with transition fixed.
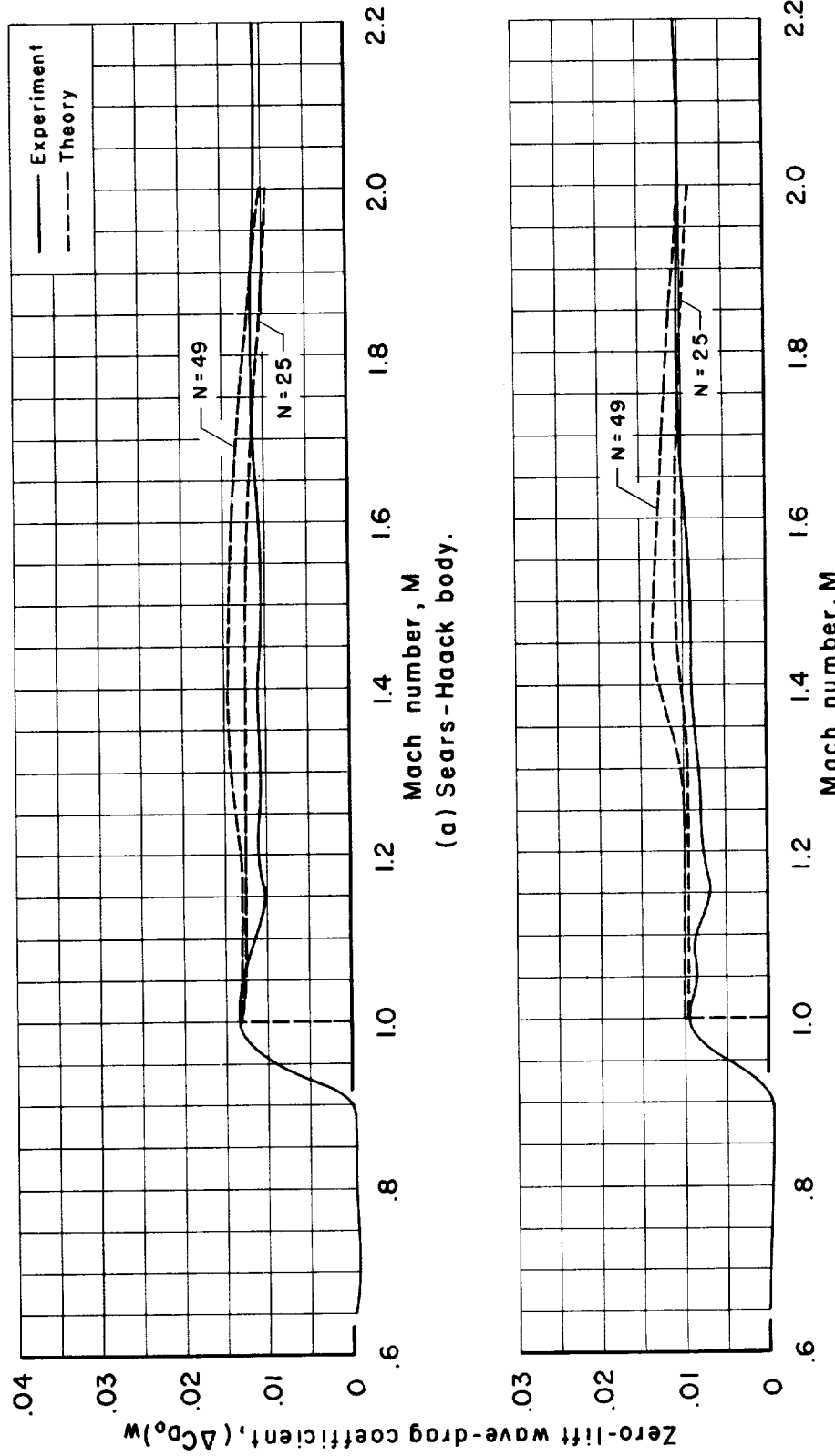
Figure 9.- Zero-lift wave-drag coefficients of the basic models with transition fixed (theory is not expected to apply for Mach numbers over $\sqrt{2}$ for these wings).

Figure 10.- Zero-lift wave-drag coefficients of the models with the thickened leading edge, transition fixed (theory is not expected to apply for Mach numbers over $\sqrt{2}$ for these wings).